Supplementary information

Solar-light-driven CO_2 reduction by methane on Pt nanocrystals partially embedded in mesoporous CeO_2 nanorods with high light-to-fuel efficiency

Mingyang Mao, Qian Zhang, Yi Yang, Yuanzhi Li,* Hui Huang, Zhongkai Jiang, Qianqian Hu, Xiujian Zhao

State Key Laboratory of Silicate Materials for Architectures (Wuhan University of Technology), 122 Luoshi Road, Wuhan 430070, P. R. China. Email: liyuanzhi66@hotmail.com

Experimental.

Preparation. mesoporous CeO_2 nanorods (denoted as CeO_2-MNR) was prepared according to the following procedure: 15.00 g of $Ce(NO_3)_3 \cdot 6H_2O$ was disolved in 20 mL of distilled water. 6.24 g of urea was dissolved in 20 mL of distilled water. The $Ce(NO_3)_3$ and urea soltuion were mixed in a telflon bottle, which was sealed tightly in a stainless steel autoclave. The autoclave was placed in electric oven, kepted at 120 °C for 16 h. After cooled to ambient temperature, the obtained precipitate was filtered, washed with distilled water, and dried at 90 °C. The obtained powder was placed in a muffle furnace, and kept at 400 °C for 4 h.

The Pt/CeO_2 nanocomposite was prepared according to the following procedure. A total of 1.50 g of CeO_2-MNR was added to 15 mL of distilled water in a beaker, and ultrasonicated for ~15 min. 3.864 g of 6.413 g L^{-1} $Pt(NO_3)_2$ aqueous solution was added to the CeO_2 suspension, uniformly mixed, and dried at 90 °C in an electric oven. The dried powder was grounded, and added to 40 mL of 1.25 g L^{-1} $NaBH_4$ aqueous solution in a beaker. After the reduction, the mixture was filtered, washed with distilled water, and dried at 90 °C for 24 h. The obtained Pt/CeO_2 sample is denoted as Pt/CeO_2-MNR. The loading of Pt in Pt/CeO_2-MNR is 1.0 wt%.

The Pt/CeO_2 nanocomposite with a lower Pt loading of 0.5 wt%, denoted as Pt-L/CeO_2-MNR, was prepared according to the same procedure as that of the Pt/CeO_2-MNR sample except for the addition of 1.932 g of 6.413 g L^{-1} $Pt(NO_3)_2$ aqueous solution to the suspension of CeO_2-MNR.

The Pt/CeO_2 nanocomposite of Pt nanoparticles supported on CeO_2 nanoparticles with 1.0 wt% Pt loading (denoted as Pt-/CeO_2-NP) was prepared according to the same procedure as that of the Pt/CeO_2-MNR sample except for the addition of a CeO_2 nanoparticle sample instead of the CeO_2-MNR sample. The CeO_2 nanoparticle sample was prepared according to the procedure as follows. A total of 15.00 g of

$Ce(NO_3)_3\cdot 6H_2O$ was disolved in 40 mL of distilled water. 10 wt% of NaOH solution was dropwise added to the $Ce(NO_3)_3$ soltuion under magnetic stirring until the pH value of the mixture was ~7. The obtained precipitate was filtered, washed with distilled water, and dried at 120 ^oC. The obtained powder was placed in a muffle furnace, and kept at 400 ^oC for 4 h.

The Pt/Al_2O_3 nanocomposite of Pt nanoparticles supported on mesoporous Al_2O_3 with 1.0 wt% Pt loading (denoted as Pt/ Pt/Al_2O_3) was prepared according to the same procedure as that of the Pt/CeO_2-MNR sample except for the addition of a mesoporous Al_2O_3 sample instead of the CeO_2-MNR sample. The mesoporous Al_2O_3 sample was prepared according to the the precedure as follows. A total of 15.00 g of $Al(NO_3)_3\cdot 9H_2O$ was disolved into 50 mL of distilled water in a beaker. 4.45 wt% amonia aqueous solution was dropwise added to the $Al(NO_3)_3$ aqueous solution under magnetic stirring until the pH value of the mixture is ~7. The beaker with the mixed solution was placed in an electric oven, heated to 90 ^oC, and then kept at 90 ^oC for 24 h. The resultant precipitate was filtered, washed with distilled water, dried at 180 ^oC for 12 h, and finally calcined at 800 ^oC for 4h.

Characterization. X-ray power diffraction (XRD) patterns of the samples were obtained by using a Rigaku Dmax X-ray diffractometer with Cu Kα radiation. SEM images were obtained on ULTRA PLUS-43-13 scanning electron microscope. Transmission electron microscopy (TEM) images were obtained on a JEM-ARM200F electron microscope (JEOL). The specific surface area of the samples was measured on Micromeritics ASAP2020 instrument using N_2 adsorption at –196 ^oC. The valence states of Pt and Ce in the Pt/CeO_2-MNR sample were examined by XPS on an ESCALAB 250Xi X-ray photoelectron spectrometer (ThermoFisher Scientific) with Mg Kα radiation. UV-Vis-IR diffusive reflectance spectra of the samples were obtained on a UV-Vis-NIR spectrophotometer (UV-3600, Shimadzu) equipped with an integrating sphere attachment. Thermogravimetric-mass spectrometry (TG-MS) analysis of the used samples was carried out on a thermogravimetric analyzer (Netzsch STA449FS/3/G) linked to a mass spectrometer (QMS403). Raman spectra of the samples were obtained on a Renishaw inVia Raman microscope by using 514.5 nm excitation. CO temperature-programmed reduction (CO-TPR) of the samples was conducted in a quartz tube reactor with a quartz window linked at one end of the reactor on TP5080 multifunctional adsorption apparatus (Tianjing Xianquan industrial and trading Co. Ltd.).

The sizes of every Pt nanocrystals in the HADDF-STEM images of the samples of Pt/CeO_2-MNR

(Figure 1E), Pt-L/CeO_2-MNR (Figure S5C), Pt/Al_2O_3 (Figure S9C), and Pt/CeO_2-NP (Figure S12C) were measured. The size distribution of Pt nanocrystals in the samples is calculated according to the formula as follows: Distribution% $= N_i/N_T \times 100\%$

Where N_i is the number of Pt nanocrystals in a known range of Pt nanocrystal sizes (e.g. 0.5~1.5 nm, 1.5~2.5 nm, etc.), N_T is the total number of all Pt nanocrystals in the HADDF-STEM image of the sample.

Photothermocatalytic activity. The catalytic activity of the catalysts for CRM under the focused irradiation from a 500 W Xe lamp (CHF-XM500, Beijing perfectlight technology Co. Ltd.) as a light source was performed on a cylindrical stainless steel gas-phase reactor with a quartz window (55.0 mm in diameter) as illustrated in Scheme S1 (*Supplementary information*). The irradiation from the Xe lamp has a spectral profile with emission across the full solar spectrum region from 200 to 2400 nm.[37] 0.0500 g of the samples was put in a sample holder of thermal insulation aluminum silicate fiber that was placed in the reactor. The irradiation from the Xe lamp was focused through the quartz window into the reactor. A feed stream of 10.2 vol% CH_4, 10.2 vol% CO_2, and Ar as balance gas was fed into the reactor. The flow rate of the feed stream, controlled by using a S49-31/MT mass flow meter (Beijing Horiba Metron instruments Co. Ltd.), was accurately measured by a soap bubble flow meter. The flow rate of the feed stream was 120.5 mL min^{-1}. A thermocouple was closely contact to the samples to measure the temperature under the focused irradiation from the Xe lamp. The effluent reactants and products were analyzed by a gas chromatograph (GC-9560, Shanghai Huaai chromatography analysis Co. Ltd.) equipped with a TDX-01 packed column, a methane convertor, thermal conductivity detector (TCD), TCD, and a flame ionization detector (FID) as schematically illustrated in Scheme S2. The irradiation power focused into the reactor from the Xe lamp was measured by an optical power meter (Newport 1918-R) connected to a thermopile sensor (Newport 818P-001-12), which was calibrated by AM 1.5 global solar light with a standard Si solar cell (Newport). The detailed procedure of the calibration and the irradiation power measurement is as follows.

The standard Si solar cell (Newport) was used to accurately measure the light intensity of the irradiation from a solar simulator equipped with air mass 1.5 global filters (1 Kw, 4×4 inch, 1000 W, Newport). The light intensity value shown by the standard Si solar cell was denoted as $I_{Si,\ AM1.5}$. At the same time, the light intensity of the irradiation from the solar simulator was also measured by the optical power meter (Newport 1918-R) connected to a thermopile sensor (Newport 818P-001-12). The light intensity value shown by the thermopile sensor was denoted as $I_{\text{thermopile, AM1.5}}$. From the values of I_{Si} and $I_{\text{thermopile}}$, the calibration coefficient of light intensity for the thermopile sensor (denoted as c) was obtained:

$$c = I_{\text{Si,AM1.5}}/I_{\text{thermopile, AM1.5}}$$

The parallel light beam from a 500 W Xe lamp system (CHF-XM500, Beijing perfectlight technology Co. Ltd.) has a circular irradiation area with a diameter of 40 mm (Scheme S1). Considering the non-uniformity of the light intensity on the circular irradiation area, the light intensities at the different positions of the circular irradiation area for the parallel light beam were measured by the thermopile sensor. The total power (W) on the circular irradiation area was calculated according to the following equation:

$$P_{\text{irradiation}}=\sum I_{\text{i}}\times c\times S_{\text{i}}$$

where I_{i} (W cm^{-2}) is the light intensity at a known position (i) with an area of S_{i} (cm^2) in the circular irradiation area.

Considering the slight attenuation of light intensity due to the transmission of the light beam from the Xe lamp through the quartz window of the reactor to the catalyst sample (Scheme S1), a quartz window the same as that of the reactor was placed between the Xe lamp and the thermopile sensor when the I_{i} values were measured.

When we measured photothermocatalytic activity of the Pt/CeO_2 sample under the focused irradiation from the Xe lamp without using any additional heater, the light beam from the Xe lamp was completely focused on the Pt/CeO_2 sample in the reactor (Scheme S1) by controlling the optical lens in the Xe lamp system. Therefore, the $P_{\text{irradiation}}$ value was used to calculate the light-to-fuel efficiency.

The irradiation power of the focused full solar spectrum irradiation was 7.3 W. As the focused irradiation area (diameter, 5 mm) on the catalyst sample is 0.19625 cm^2, the irradiation intensity is 371.1 kW m^{-2} (corresponding to 371.1 suns). In order to measure the catalytic activity of the Pt/CeO_2-MNR sample for CRM under the focused irradiation of visible-infrared light form the Xe lamp, a long-wave pass cutoff filter was placed between the Xe lamp and the quartz window. The irradiation power of the focused visible-infrared irradiation with wavelength above 420, 560, or 690 nm was 6.1, 5.3, or 4.0 W, respectively. The corresponding irradiation intensity is 311.4, 269.9, or 197.3 kW m^{-2}, respectively.

The light-to-fuel efficiency *(η)* is defined as:[1]

$\eta = (r_{H2} \times \Delta_c H^0_{H2} + r_{CO} \times \Delta_c H^0_{CO} - r_{CH4} \times \Delta_c H^0_{CH4})/P_{irradiation}$ (1)

The standard heat of combustion ($\Delta_c H^0$, 298.15 K) or higher heating value for the H_2, CO, and CH_4 fuels ($\Delta_c H^0_{H2}$, $\Delta_c H^0_{CO}$, and $\Delta_c H^0_{CH4}$) is 285.8, 283.0, and 890.8 kJ mol^{-1},[S1] respectively (*Note*: CO_2 is not a fuel, its $\Delta_c H^0$ is 0), and $P_{irradiation}$ is the irradiation power focused into the reactor from the Xe lamp.

Under the focused irradiation from the Xe lamp (full solar spectrum from 240 to 2400 nm,[37] the power of the focused irradiation into the reactor: 7.3 W), the production rates of H_2 and CO (r_{H2} and r_{CO}) are 287.1 and 302.1 umol min^{-1}, respectively. The reaction rates of CH_4 and CO_2 (r_{CH4} and r_{CO2}) are 137.8 and 156.9 umol min^{-1}, respectively. The η is calculated to 10.3%. The η under the focused visible-infrared irradiation with wavelength above 420, 560, or 690 nm, which is calculated by similar procedure, is 10.2%, 10.2%, or 10.6%, respectively.

The η is also calculated according to the following equation based on the standard molar Gibbs energy of formation ($\Delta_f G°$, 298.15 K) for the reactants and products:

$\eta = (r_{H2} \times \Delta_f G^0_{H2} + r_{CO} \times \Delta_f G^0_{CO} - r_{CH4} \times \Delta_f G^0_{CH4} - r_{CO2} \times \Delta_f G^0_{CO2})/P_{irradiation}$ (2)

The standard molar Gibbs energy of formation of H_2, CO, CH_4, and CO_2 ($\Delta_f G^0_{H2}$, $\Delta_f G^0_{CO}$, $\Delta_f G^0_{CH4}$, $\Delta_f G^0_{CO2}$) is 0, -137.2, -50.5, and -394.4 kJ mol^{-1},[S1] respectively. Under the focused irradiation from the Xe lamp, the η is calculated to 6.3% according to equation (2), which is lower to the η value (10.3%) according to the equation (1) based on the standard heat of combustion for the H_2, CO, and CH_4 fuels.[1] The η under the focused visible-infrared irradiation with wavelength above 420, 560, or 690 nm according to the equation (2), which is calculated by similar procedure, are 6.7%, 7.3%, or 7.0%, respectively. The η value based on the Gibbs energy lower than the corresponding that based on the heat of combustion (enthalpy) is attributed to the fact that ΔG_{298} of CRM (170.5 kJ mol^{-1}) is lower than its ΔH_{298} (247 kJ mol^{-1}) because CRM is a reaction of entropy increase ($\Delta S_{298} = 256.6$ J K^{-1} mol^{-1}), resulting in an energy consumption according to the Gibbs free energy equation ($\Delta G = \Delta H - T \times \Delta S$).

When we measured the photothermocatalytic activity of the Pt/CeO_2 sample for CRM under the focused irradiation from the Xe lamp, a feed stream of 10.2 vol% CH_4, 10.2 vol% CO_2, and Ar as balance gas was fed into the reactor (*see Figure 2, Experimental*). The use of inert gas (Ar) as a balance gas or diluting gas is not necessary for the catalytic CRM reaction on the Pt/CeO_2 samples to proceed. We used the inert gas as diluting gas just for the safety consideration as high concentration CH_4 gas is dangerous in laboratory. Even so, we still consider the power required to separate the diluting inert gas from air, and calcluated the light-to-fuel efficiency *(η)* for solar-light-driven CRM according to the equation and procedure the same as those reported by Chueh *et al.*[1]:

$\eta = (r_{H2} \times \Delta_c H^0_{H2} + r_{CO} \times \Delta_c H^0_{CO} - r_{CH4} \times \Delta_c H^0_{CH4})/(P_{\text{irradiation}} + r_{\text{inert}} \times E_{\text{inert}})$ (3)

where r_{inert} is the flow rate of the inert gas, and E_{inert} is the energy required to separate the inert gas from air.

For the photothermocatalytic CRM on the Pt/CeO_2-MNR sample under the focused irradiation (full solar spectrum) from the Xe lamp (Figure 2), the reaction rates of CH_4 and CO_2 (r_{CH4} and r_{CO2}) are 137.8 and 156.9 umol min^{-1}, respectively. The flow rate of the inert gas (Ar) is 3926.0 umol min^{-1}. The production rates of H_2 and CO (r_{H2} and r_{CO}) are 287.1 and 302.1 umol min^{-1}, respectively. In this case, we take E_{inert} to be 20 kJ mol^{-1} (*the energy required to separate N_2 from air*), the same as that used in the literature,[1] as N_2 as diluting gas has the same function as Ar. The η value is calculated to be 8.7%. The η value under the focused visible-infrared irradiation with wavelength above 420, 560, or 690 nm, which is calculated by similar procedure, is 8.4%, 8.1%, or 8.0%, respectively.

Note: In the solar-driven thermochemical dissociation of CO_2 and H_2O using nonstoichiometric ceria reported by Chueh *et al.*[1] the solar-to-fuel efficiency is calculated according to the following equation:

$\eta = r_{\text{fuel}} \times H_{\text{fuel}} /(P_{\text{solar}} + r_{\text{inert}} \times E_{\text{inert}})$

where r_{fuel} is the molar fuel production rate, ΔH_{fuel} is the higher heating value of the fuel (H_2 or CO), P_{solar} is the incident solar radiation power, r_{inert} is the flow rate of the inert gas during oxygen evolution, and E_{inert} is the energy required to separate the nitrogen sweep gas from air (20 kJ mol^{-1}, in the work, Ar was utilized as the sweep gas instead of N_2 purely for reasons of experimental convenience [1]).

They considered the power required to separate the inert sweep gas from air. Their consideration is necessary because they realized solar-driven thermochemical dissociation of CO_2 and H_2O by the following two steps:[1]

Step 1: CeO_2=CeO_{2-x}+0.5xO_2 (at high temperature 1420°~1640 °C)

Step 2: CeO_{2-x}+xH_2O=CeO_2+xH_2 or CeO_{2-x}+xCO_2=CeO_2+xCO (at relatively lower temperature ~900°C)

It is necessary to use inert gas (e.g. Ar or N_2) as sweep gas to remove the produced O_2 in the *step 1*, otherwise, the reaction of ceria decomposition cannot proceed because the produced oxygen can oxidize the reduced ceria (CeO_{2-x}) to CeO_2. Thus, the power required to separate the inert sweep gas from air must be considered in the calculation of solar-to-fuel efficiency in the literature.[1]

Photocatalytic activity. The catalytic activity of Pt/CeO_2-MNR for CRM at near ambient temperature under the irradiation from the Xe lamp was tested on a cylindrical stainless steel gas-phase reactor with a quartz window (55 mm in diameter). 0.0500 g of Pt/CeO_2-MNR was coated on a glass slide, which was placed on the bottom of the reactor. The reactor was put in an ice-water bath for maintaining the reaction temperature at near ambient temperature under the irradiation of the Xe lamp. The light intensity of the irradiation is 4.7 kW m^{-2}. The other procedure is the same as that for measuring the photothermocatalytic activity.

Thermocatalytic activity.The thermocatalytic activity of Pt/CeO_2-MNR for CRM at different temperatures was performed at atmospheric pressure on a WFS-2015 online gas-phase reaction apparatus (Tianjing Xianquan industrial and trading Co. Ltd.) in a flow fixed-bed quartz tubular reactor (7.5 mm in inner diameter and 300.0 mm in length). The reactor was placed in an electric tubular furnace. A mixture of 0.0250 g of the Pt/CeO_2-MNR sample diluted by 0.25 g of quartz powder was put in the middle of quartz tubular reactor supported by quartz wool. A thermocouple was inserted into the reactor to closely contact to the sample for measuring reaction temperature. A feed stream of 10.0 vol% CH_4, 10.4 vol% CO_2, and Ar as balance gas was continuously fed into the reactor. The flow rate of the feed stream is 10.2 mL min^{-1}.

In situ FTIR. In situ FTIR spectra of the reactants of CH_4 or CO_2 adsorbed on the samples at different temperatures were recorded on a Nicolet-6700 infrared spectrometer (ThermoFisher Scientific) equipped with a reaction chamber (Harrick). The sample was uniformly put on the sample stage incorporated in a cartridge heater with a thermocouple in the reaction chamber. The sample was pretreated in a flow of high purity N_2 at a flow rate of 30 mL min^{-1} at 120 °C for 30 min. After cooling to ambient temperature, the background of the FTIR spectra was taken. The carrier gas was changed to a flow of 30 mL min^{-1} high purity CH_4 (purified with O_2 absorbent, Fe/SiO_2) for 10 min. The FTIR spectra of CH_4 adsorbed on the sample were recorded at ambient temperature. Then, the sample was heated to a known temperature (e.g. 200, 250, 300, 350, 400, 450, 500 °C), and the FTIR spectra were recorded at each temperature. After that, the reaction chamber was cooled to ambient temperature. The carrier gas was changed to a flow of 30 mL min^{-1} high purity CO_2 (purified with O_2 absorbent, Fe/SiO_2) for 10 min. The FTIR spectra of CO_2 adsorbed on the sample were recorded at ambient temperature. Then, the sample was heated to a known temperature (e.g. 200, 250, 300, 350, 400, 450, 500 °C), and the FTIR spectra were recorded at each temperature.

Isotope labeling of thermocatalytic CRM: Isotope labeling experiment of thermocatalytic CRM on the Pt/CeO_2-MNR sample was performed on a setup schematically illustrated in Scheme S3 according to the procedure as follows: A flow fixed-bed quartz tubular reactor was connected through a micro pump to a quartz tubular gas cell with two CaF_2 windows, which was placed in a Nicolet-6700 infrared spectrometer. 0.0500 g of the Pt/CeO_2-MNR sample was placed in the quartz tubular reactor. The experiment system was pre-purged with high purity N_2. A feed stream of 20 mL of $^{12}CH_4$, 10 mL of $^{12}C^{18}O_2$ (Aldich), and 270 mL of N_2 as balance gas was introduced into the system by the corresponding gas bags, which were conected to the system. After the reactor was heated to 700 ^{o}C, the micro pump was turned on. The reaction of $^{12}CH_4$ and $^{12}C^{18}O_2$ started to take place. FTIR spectra of the reactants and products were recorded.

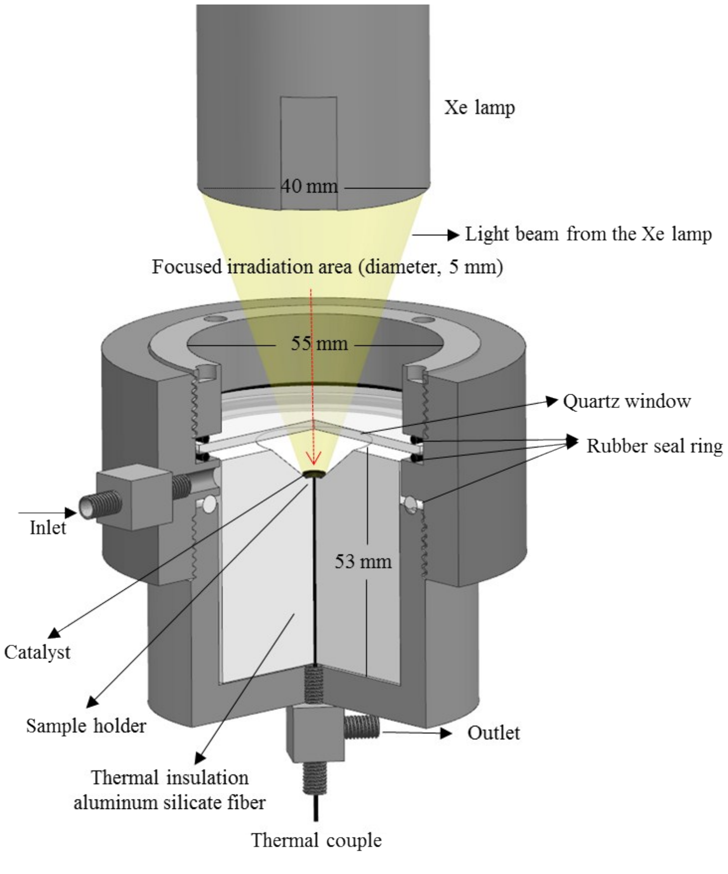

Scheme S1. The schematic illustration of the reactor for measuring the catalytic activity of the samples under the focused irradiation from the Xe lamp without using additional electric heater.

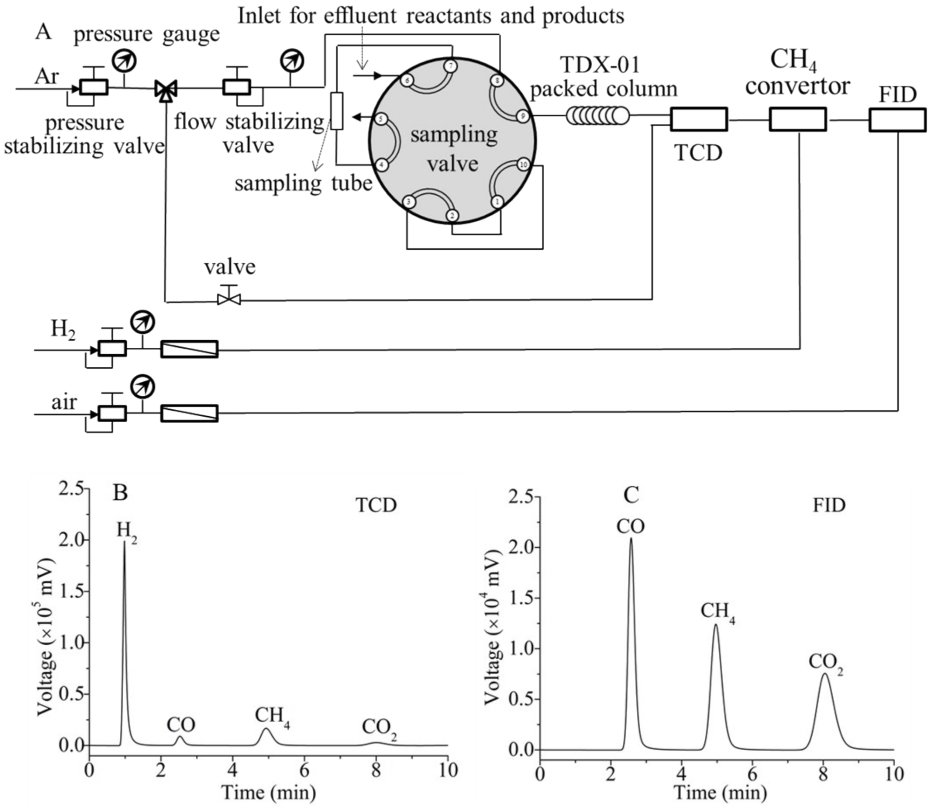

Scheme S2. Schematic chart for the analysis of the effluent reactants and products by gas chromatography (A). Typical GC spectra for the analysis of H_2 by a thermal conductivity detector (TCD) (B). Typical GC spectra for the analysis of CO, CH_4, and CO_2 by a flame ionization detector (FID)(C): The effluent reactants and products flow into a TDX-01 packed column through a sampling valve, a thermal conductivity detector (TCD) using Ar as carrier gas, a CH_4 convertor, and a flame ionization detector (FID). H_2 in the effluents is analyzed by TCD. CO and CO_2 in the effluents are converted to CH_4 in the CH_4 convertor using Ni/SiO_2 as the catalyst. The gases of CO (converted to CH_4), CH_4, and CO_2 (converted to CH_4) in the effluents are analyzed by FID. Actually, the gases of CO, CH_4, and CO_2 in the effluents can be also analyzed by TCD as shown in Scheme 2B. As FID has higher sensitivity to CH_4, we use FID to analyze the gases of CO, CH_4, and CO_2.

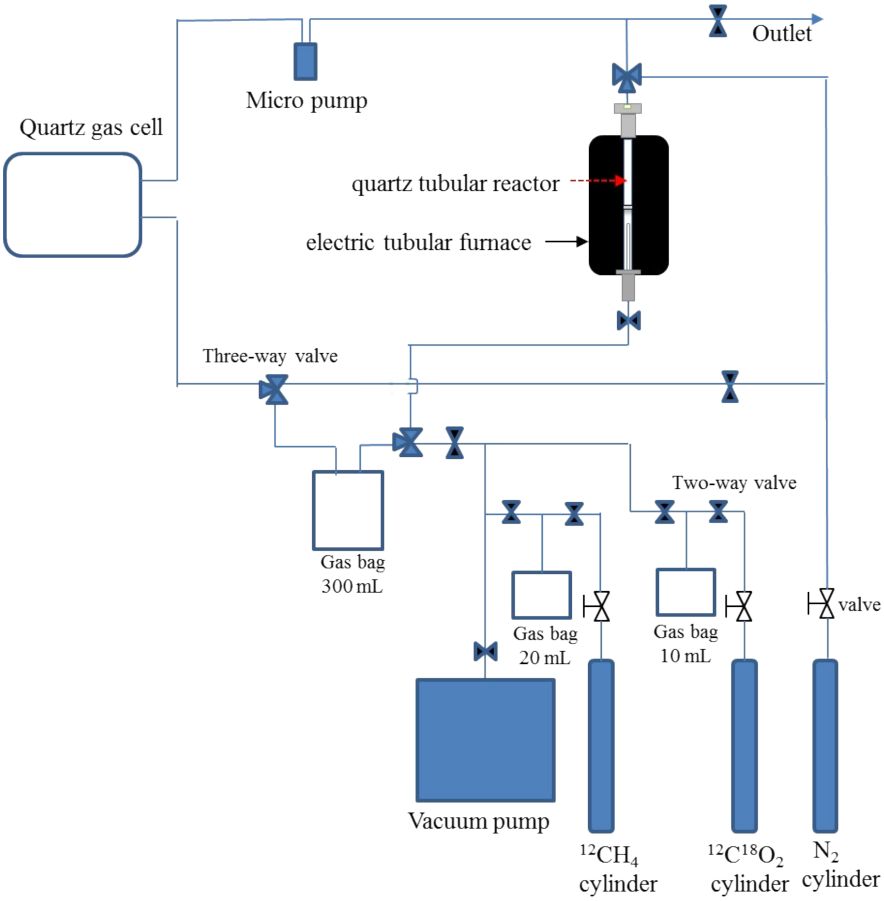

Scheme S3. Schematic illustration of the setup for isotope labeling experiment in which $^{12}C^{18}O_2$ reacts with $^{12}CH_4$ on the Pt/CeO_2-MNR sample.

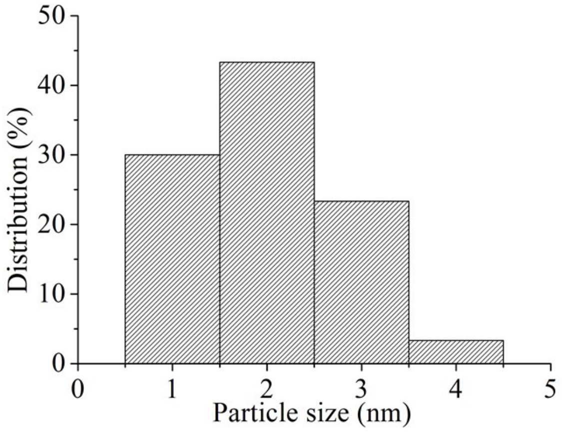

Figure S1. The size distribution of Pt nanocrystals in Pt/CeO_2-MNR.

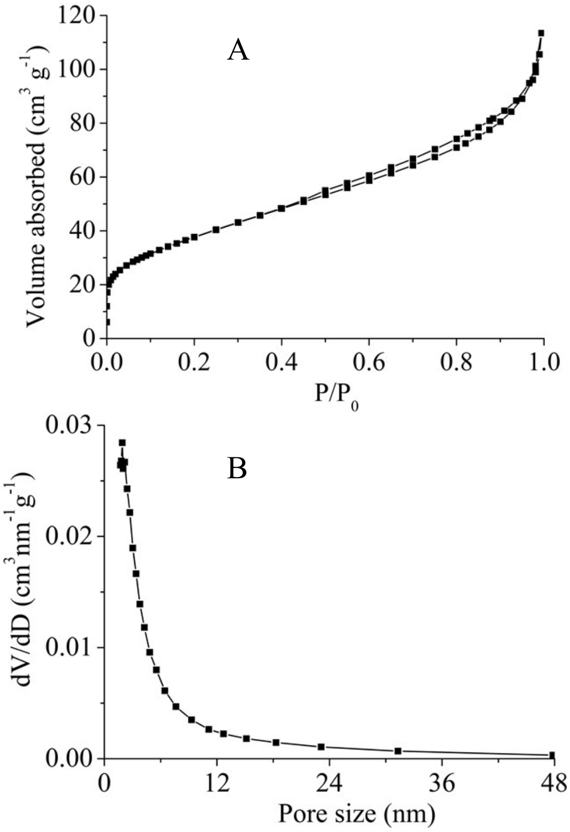

Figure S2. N_2 adsorption/desorption isotherms (A) and BJH adsorption pore size distribution (B) of Pt/CeO_2-MNR.

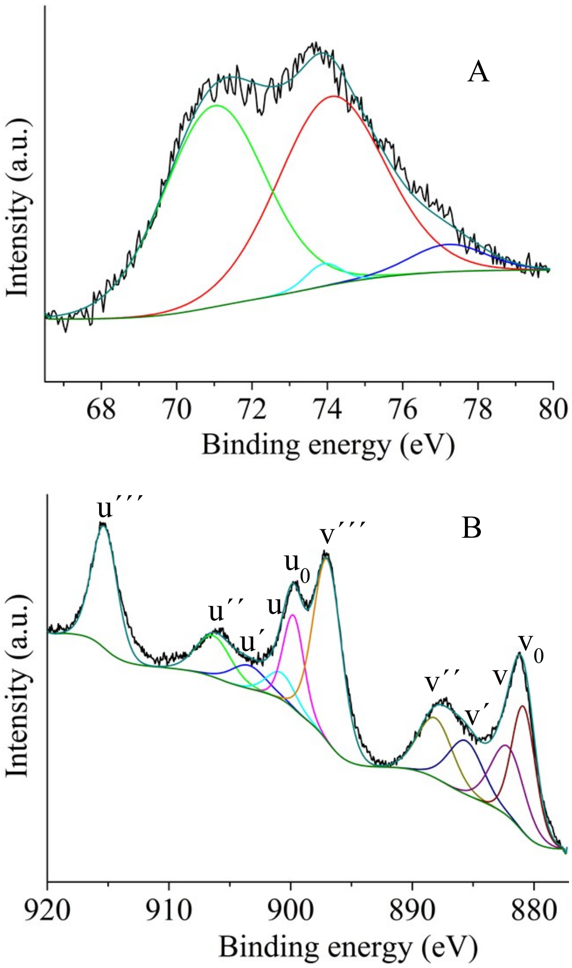

Figure S3. Pt 4f (A) and Ce 3d (B) spectra of Pt/CeO$_2$-MNR.

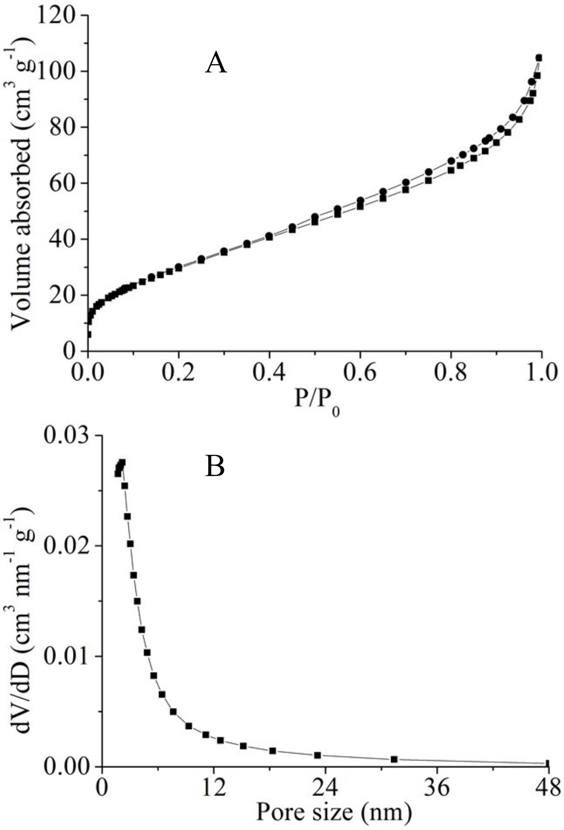

Figure S4. N_2 adsorption/desorption isotherms (A) and BJH adsorption pore size distribution (B) of Pt-L/CeO_2-MNR.

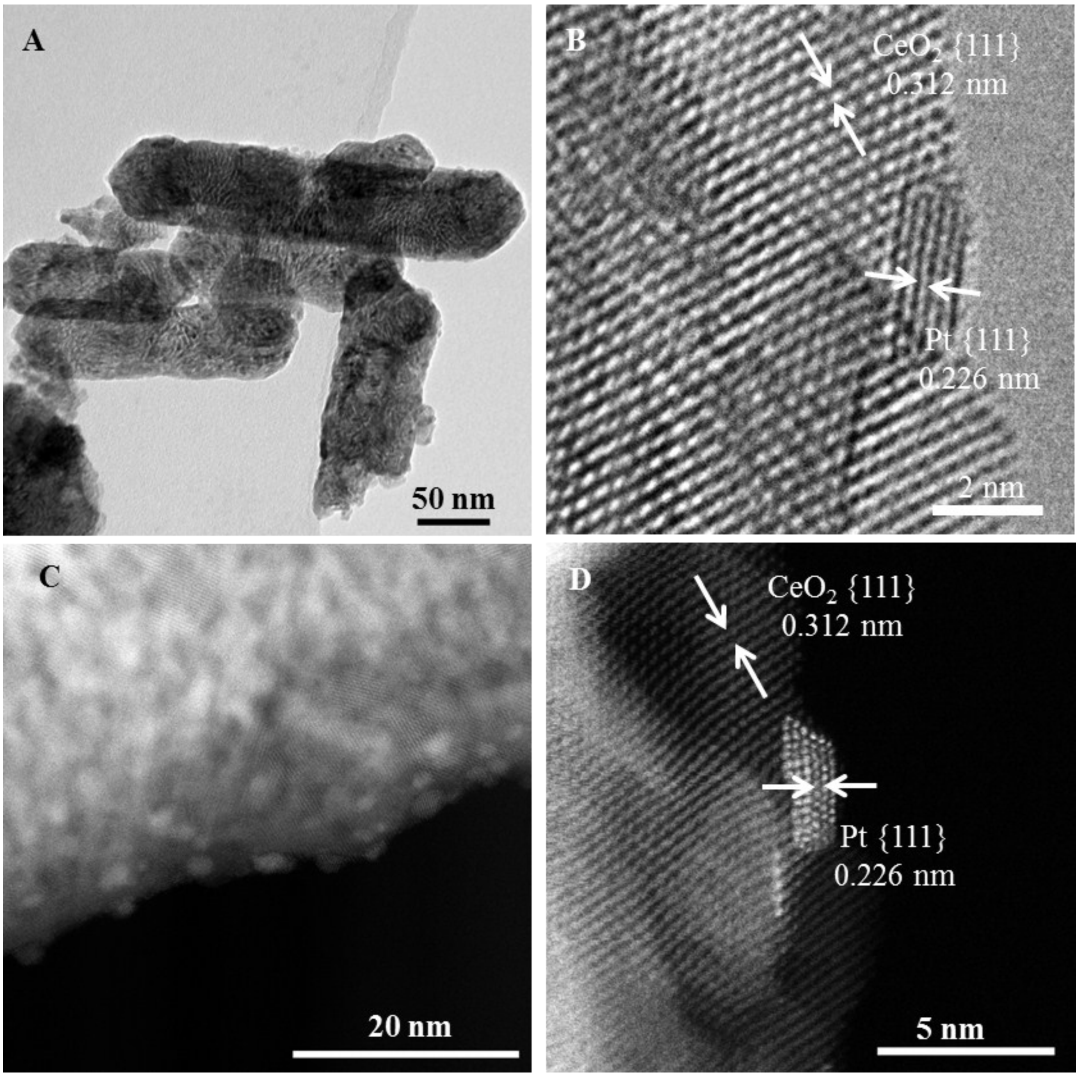

Figure S5. TEM (A), HRTEM (B), HADDF-STEM (C), and high resolution HADDF-STEM (D) of Pt-L/CeO$_2$-MNR.

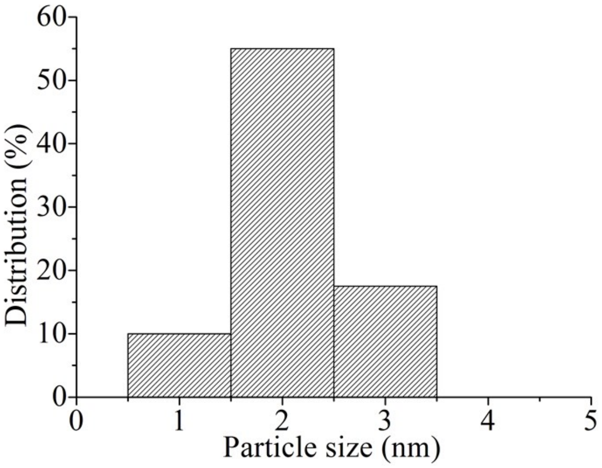

Figure S6. The size distribution of Pt nanocrystals in Pt-L/CeO$_2$-MNR.

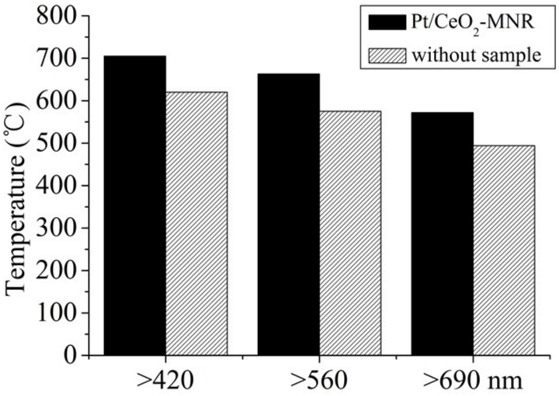

Figure S7. The T_{eq} values of the Pt/CeO$_2$-MNR sample and the sample holder surface under the focused irradiation of visible-infrared light from the Xe lamp.

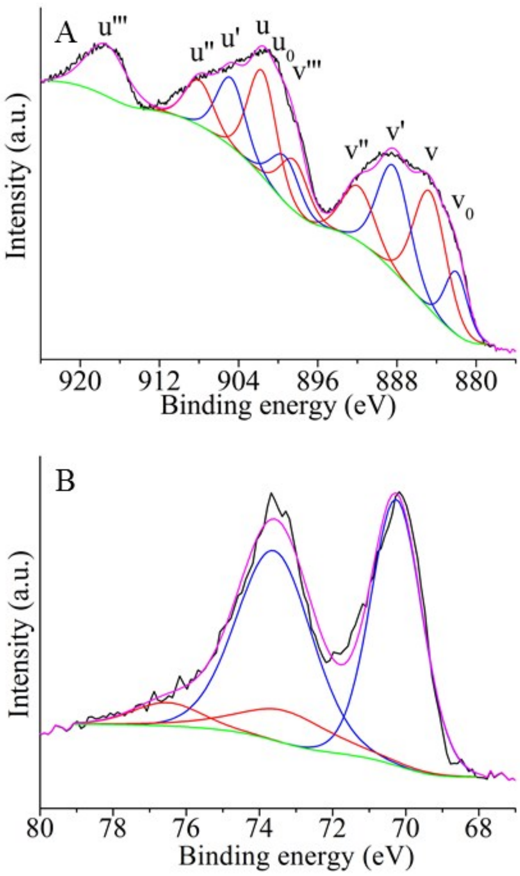

Figure S8. Ce 3d (A) and Pt 4f (B) spectra of the used Pt/CeO$_2$-MNR sample. The Pt$_{4f}$ XPS spectra are fitting into two sets of spin-orbit doublets of Pt 4f$_{7/2}$ and Pt 4f$_{5/2}$ (Fig. S8B). The peaks around 70.2 and 73.7 eV are assigned to Pt 4f$_{7/2}$ and Pt 4f$_{5/2}$ of metallic Pt, while the peaks around 73.3 and 76.5 eV are assigned to Pt 4f$_{7/2}$ and Pt 4f$_{5/2}$ of Pt^{4+}.[33, 34] The molar ratio of Pt^{4+}/Pt^0 is estimated to be 0.17. The presence of the small amount of Pt^{4+} is ascribed to the chemisorption of oxygen on the surface of Pt nanocrystals due to the exposure of the used Pt/CeO$_2$-MNR sample in air. Compared to those of Pt in the fresh Pt/CeO$_2$-MNR sample (Fig. S3A), the Pt 4f$_{7/2}$ and Pt 4f$_{5/2}$ peaks of Pt in the used Pt/CeO$_2$-MNR sample obviously shift from 71.0 and 74.3 eV to lower binding energies of 70.2 and 73.7 eV, respectively. This is attributed to the increase in the amount of Ce^{3+} species at the Pt/CeO$_2$ interface as the ionization potential of Ce^{3+} is lower than that of Ce^{4+}.[44]

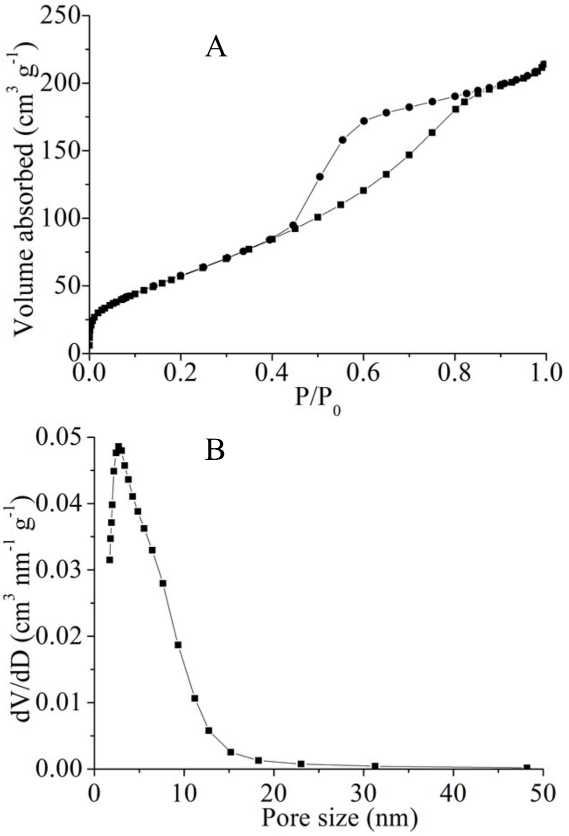

Figure S9. N_2 adsorption/desorption isotherms (A) and BJH adsorption pore size distribution (B) of Pt/Al_2O_3.

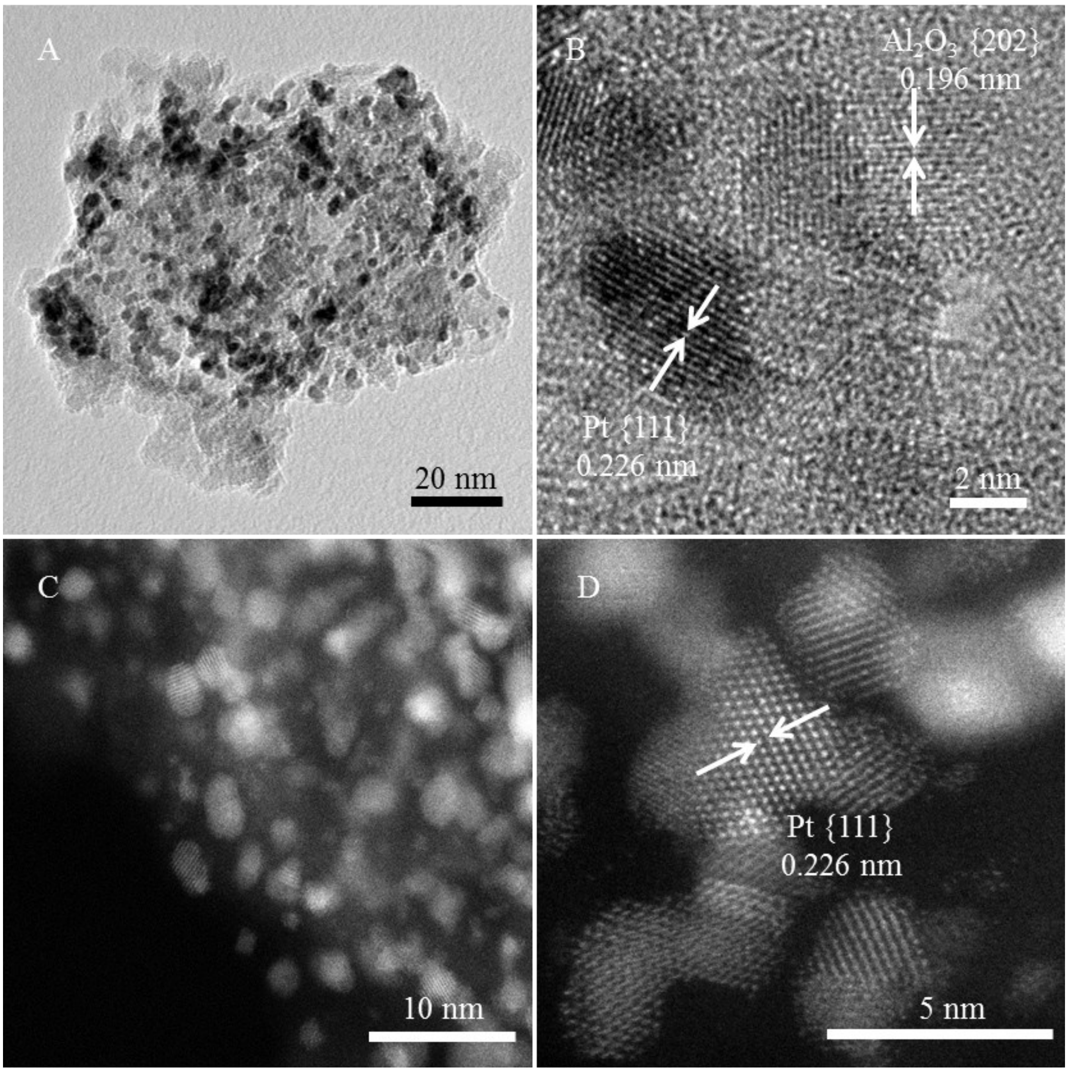

Figure S10. TEM (A), HRTEM (B), HAADF-STEM (C), and high resolution HAADF-STEM (D) of Pt/Al_2O_3.

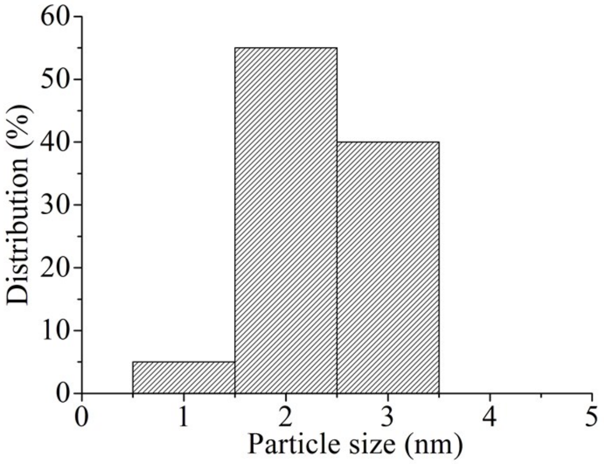

Figure S11. The size distribution of Pt nanocrystals in Pt/Al_2O_3.

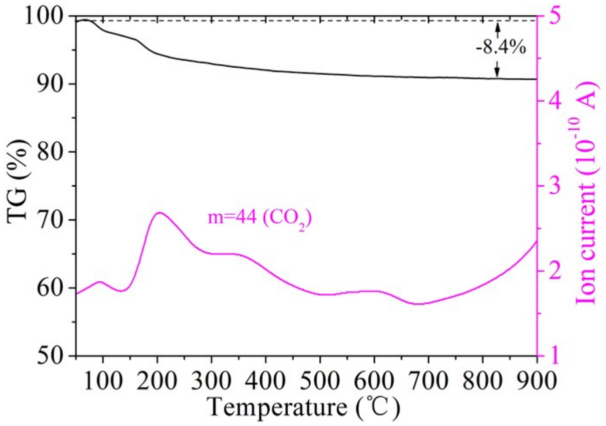

Figure S12. TG-MS profiles of the used Pt/Al_2O_3 catalyst.

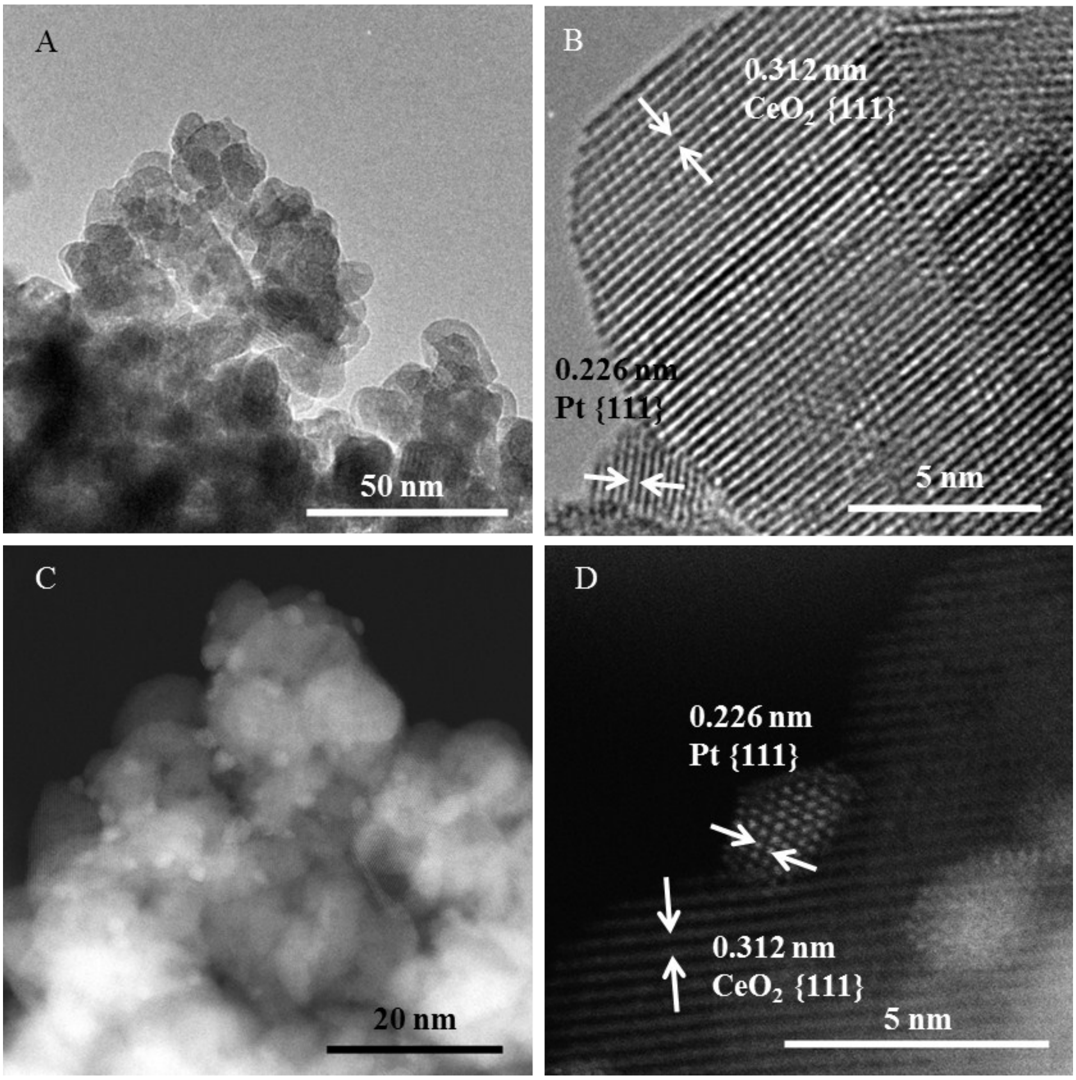

Figure S13. TEM (A), HRTEM (B), HADDF-STEM (C), and high resolution HADDF-STEM (D) of Pt/CeO_2-NP.

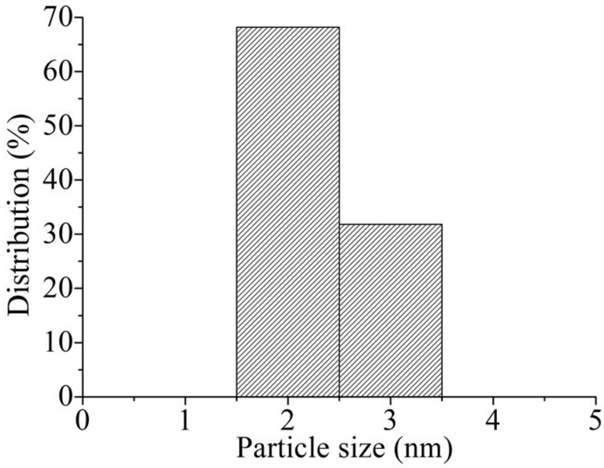

Figure S14. The size distribution of Pt nanocrystals in Pt/CeO_2-NP.

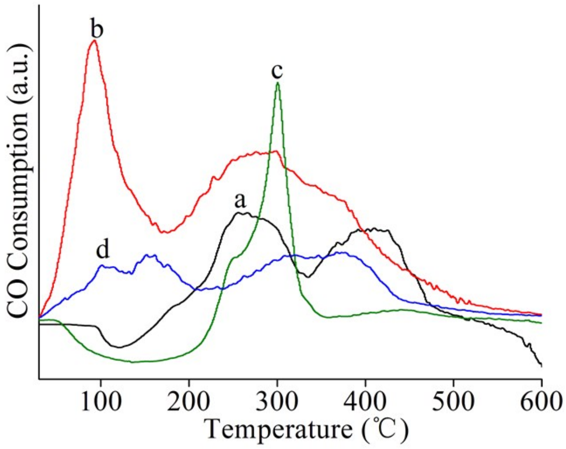

Figure S15. The profiles of the temperature-programmed reduction of the samples by CO: CeO_2-MNR (a), Pt/CeO_2-MNR (b), CeO_2-NP (c), and Pt/CeO_2-NP (d).

CeO_2-MNR has two strong CO consumption peaks around ~265, ~410 °C, which are attributed to the oxidation of CO by two types of surface lattice oxygen of CeO.[33, S2, S3] Compared to CeO_2-MNR, the partial confinement of Pt nanoparticles in mesoporous CeO_2 (Pt/CeO_2-MNR) leads to a strong TPR peak around a much lower temperature of ~91 °C. This observation indicates that more active oxygen is produced by the partial confinement of Pt nanoparticles in mesoporous CeO_2 due to the metal-support interaction, which makes oxygen of CeO_2 at the Pt/CeO_2 interface more active.[33] As can be seen from Fig. S14, the peaks of the surface oxygen removal for CeO_2-NP appear at higher temperatures compared to the corresponding peaks of CeO_2-MNR. This observation indicates that the surface oxygen of CeO_2-NP is less active than that of CeO_2-MNR. Compared to CeO_2-NR, Pt nanoparticles supported on CeO_2-

NP (Pt/CeO_2-NP) leads to two strong TPR peaks around ~104 and ~ 155 °C. This observation indicates that more active oxygen is produced by supporting Pt nanoparticles on CeO_2 nanoparticles due to the metal-support interaction. However, the strong peaks of Pt/CeO_2-NP appear at higher temperature than that of Pt/CeO_2-MNR (~91 ^{o}C), indicating that oxygen at the Pt/CeO_2 interface in Pt/CeO_2-NP is less active than that in Pt/CeO_2-MNR. Meanwhile, the two peaks corresponding to the active oxygen at the Pt/CeO_2 interface in Pt/CeO_2-NP is less intensive than that in Pt/CeO_2-MNR, suggesting that the amount of the active oxygen in Pt/CeO_2-NP is lower than that of Pt/CeO_2-MNR. These result in the lower catalytic activity of Pt/CeO_2-NP for CRM than that of Pt/CeO_2-MNR, as shown in Fig. 6B and 6C.

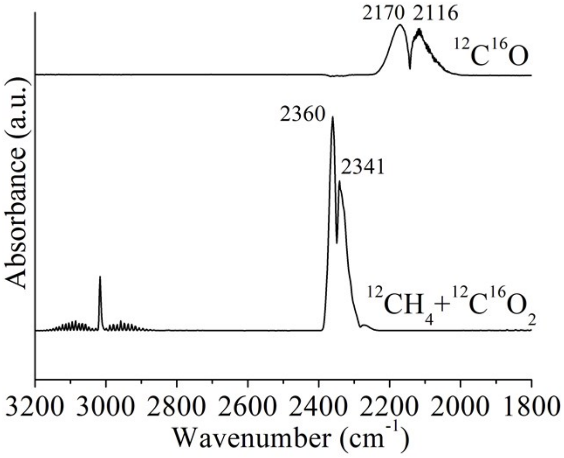

Figure S16. FTIR spectra of $^{12}C^{16}O$ gas and the gas mixture of $^{12}CH_4$ and $^{12}C^{16}O_2$.

References

S1. D. R. Lide, CRC Handbook of Chemistry and Physics, CRC Press, **2003**.

S2. Z. L. Wu, M. J. Li and S. H. Overbury, *J. Catal.*, 2012, **285**, 61−73.

S3. X. W. Liu, K. B. Zhou, L. Wang, B. Y. Wang and Y. D. Li, *J. Am. Chem. Soc.*, 2009, **131**, 3140−3141.